The Mode Mixing Problem and its Influence in the Neural Activity Reconstruction

Maximiliano Bueno-López, Eduardo Giraldo, Marta Molinas and Olav Bjarte Fosso

Abstract—**This paper presents and discusses the challenge of mode mixing when using the Empirical Mode Decomposition (EMD) to identify intrinsic modes from EEG signals used for neural activity reconstruction. The standard version of the EMD poses some challenges when decomposing signals having intermittency and close spectral proximity in their bands. This is known as the Mode Mixing problem in EMD. Several approaches to solve the issue have been proposed in the literature, but no single technique seems to be universally effective in preserving independent modes after the EMD decomposition. This paper exposes the impact of mode mixing in the process of neural activity reconstruction and reports the results of a performance comparison between a well known strategy, the Ensemble EMD (EEMD), and a new strategy proposed by the authors for mitigating the mode mixing problem. The comparative evaluation shows a more accurate neural reconstruction when employing the strategy proposed by the authors, compared to the use of EEMD and its variants for neural activity reconstruction.**

Index Terms—**EEG signals, Empirical Mode Decomposition, Mode Mixing.**

I. Introduction

THE EEG is an indicator of neural activity and is used to study cognitive processes, physiology, emotion recognition and complex brain dynamics [1], [2]. Due to the non-linear and non-stationary nature of EEG signals, they are difficult to analyze in the time and frequency domain. However, some important characteristics can be extracted to assist early detection of different disorders by using advanced signal analysis techniques [3], [4]–[6]. In recent years, the Hilbert Huang Transform (HHT) has been increasingly used in the analysis of such signals. However, in some applications, the extraction of information has been hampered by the mode mixing problem that appears in the Empirical Mode Decomposition (EMD) when frequency components are relatively close or exhibit intermittency. A mode mixing problem appears when an Intrinsic Mode Function (IMF) either consists of signals of widely disparate scales, or a signal of a similar scale resides in different IMF components.

Manuscript received July 31, 2018; revised January 21, 2019. This work was carried out under the funding of the Departamento Administrativo Nacional de Ciencia, Tecnología e Innovación (Colciencias). Research project: 111077757982 "Sistema de identificación de fuentes epileptogénicas basado en medidas de conectividad funcional usando registros electroencefalográficos e imágenes de resonancia magnética en pacientes con epilepsia refractaria: apoyo a la cirugía resectiva".

M. Bueno-López is with the Department of Electrical Engineering, Universidad de La Salle, Bogotá, Colombia, e-mail: maxbueno@unisalle.edu.co.

E. Giraldo is with the Department of Electrical Engineering, Universidad Tecnológica de Pereira, Pereira, Colombia, e-mail: egiraldos@utp.edu.co.

M. Molinas is with the Department of Engineering Cybernetics, Norwegian University of Science and Technology, Trondheim, Norway, e-mail: marta.molinas@ntnu.no

O. B. Fosso is with the Department of Electric Power Engineering, Norwegian University of Science and Technology, Trondheim, Norway, e-mail: olav.fosso@ntnu.no

The presence of mode mixing can hamper the physical interpretation of the process which is intended to be described by the individual IMFs [7], [8]. The mode mixing problem has been studied in different applications, for example in [9], where the authors discuss how the mode mixing influences the EMD-based methods for hydrocarbon detection. They use mode-mixing elimination methods, specifically ensemble EMD (EEMD) and complete ensemble EMD (CEEMD), as tools for identification of the peak amplitude above average volume and the peak frequency volume. In [10], a method was proposed based on the morphological filter to remove the noise and the revised blind source separation to deal with the mode mixing. The method was tested with vibration signals from a mechanical system. In [11], a sinusoidal-assisted EMD (SAEMD) for efficient and effective HHT computation to solve mode-mixing problems was proposed. The new tool was tested using the Global Sea Surface Temperature (GSST) application from 1856 to 2003.

In the specific case of EEG signals, the EMD and the Hilbert Huang Transform (HHT) have been used to obtain a better signal representation and to detect instantaneous frequencies [12], [13]. In [14], an approach that combines EEMD and ICA for selection of artifactual components and concentration of artifacts was presented. The effectiveness of the proposed approach was examined using semi-simulated data purposely contaminated with selected artifacts. In [15], the authors quantified the interaction between different electrodes using a nonlinear measure known as synchronization likelihood (SL) which effectively measures the synchronization between non-stationary signals like EEG. The empirical mode decomposition (EMD) is applied to decompose the EEG signal into intrinsic oscillatory modes. In other cases, the EMD is used for classification of electroencephalogram signals. The intrinsic mode functions generated have been used as an input to classifiers as least squares support vector machine (LS-SVM) [16], [17]. Based on the above, it is arguable that the use of EMD in applications involving EEG signals needs to be combined with other techniques to handle the Mode Mixing problem [13], [18]–[24].

The purpose of this paper is to contribute to a better understanding of the challenges that EMD poses when applied to EEG signals and to discuss solutions to the mode mixing problem in this specific area. With this application, the goal is to find an accurate brain reconstruction from the EEG bands decomposition. This paper is organized as follows: Section II gives an introduction to the essential concepts of EMD. The mode mixing problem and some established solutions are given in section III, and in section

(Advance online publication: 12 August 2019)

IV we propose a new methodology to solve this problem. Illustrative examples are shown in Section V, while the discussion of the results is presented in Section VI. Finally, conclusions are given in Section VII.

II. Empirical Mode Decomposition

The Empirical Mode Decomposition has been proposed as an adaptive time-frequency data analysis method [25]. The EMD does not require any restrictive assumption on the underlying model (no basic function) of the process/system under analysis and is able to handle both non-linear and non-stationary signals. However, the algorithm has shown to have some limitations in identifying closely spaced spectral tones and components appearing intermittently in the signal. The aim of the EMD method is to decompose the nonlinear and nonstationary signal $y(t_k)$ into a sum of intrinsic mode functions (IMFs) that satisfies two conditions [26]:

1) Symmetric upper/lower envelopes (zero mean).
2) The numbers of zero-crossing and extrema that are either equal or differ by exactly one.

The EMD algorithm for the signal $y(t_k)$ can be summarized as follows:

1) Identify all extrema (maxima and minima) in $y(t_k)$.
2) Interpolate between minima and maxima, generating the envelopes $e_l(t_k)$ and $e_m(t_k)$.
3) Determine the local mean as $m(t) = (e_l(t_k)+e_m(t_k))/2$.
4) Obtain the residue $r(t_k) = y(t_k) - m(t_k)$
5) Decide whether $r(t_k)$ is an IMF or not based on the two basic conditions for IMFs mentioned above.
6) Repeat step 1 to 4 until $r(t_k)$ will be monotonic.

Empirical Mode Decomposition is applied over $\boldsymbol{y}(t_k)$ to obtain $\gamma_i(t_k)$ being i the intrinsic mode function (IMF), and

$$\boldsymbol{y}(t_k) = \sum_{i=1}^{N} \gamma_i(t_k) + \boldsymbol{r}(t_k) \tag{1}$$

where N is the number of IMFs and $\boldsymbol{r}(t_k)$ a residual. Recently, some optimization techniques have been proposed to improve the performance of the EMD [27], [28].

Having obtained the intrinsic mode function components, the Hilbert transform can be applied to each component and the instantaneous frequency is found using equation (2).

$$f_i(t) \triangleq \frac{1}{2\pi} \cdot \frac{d\theta_i(t)}{dt}, \tag{2}$$

In (2), $\theta_i(t)$ is the instantaneous phase of each IMF calculated from the associated analytical signal [29]. Finally, the instantaneous frequency can be observed in the Hilbert Spectrum.

III. Mode mixing problem and its solution

Mode mixing, observed in the context of the EMD caused by either intermittency of a signal component or by spectral proximity, is a well recognized challenge of the method [7], [9], [30]. In [8] and [31], the authors address the issue of *One or Two Frequencies?*, and define a set of conditions that must exist between the frequency components of a signal to ensure that they can be recognized as independent modes in the EMD decomposition. The mode mixing problem has been analyzed in different areas. In [9], an application for hydrocarbon detection is presented, while in [10], the authors show an application in mechanical systems. In this paper, two previously known methods and one new method proposed by the authors in [23] are introduced to handle the mode mixing in the detection of signal sources from different regions of the brain. The signals are collected using EEG.

A. Masking Signal

The masking signal method reduces the problem of mode mixing when frequency components are closely spaced (in the same octave). The masking signal approach was proposed in [30]. The basic idea is to add a new signal to the analyzed signal. This signal will prevent lower frequency components from being mixed together with the higher frequencies in the same IMFs. Since the masking signal is known, it can be removed from the IMF following the procedure indicated below:

1) Construct a masking signal $s(n)$, from the frequency information of the original data, $y(t_k)$.
2) Perform EMD on $y_+(t_k) = y(t_k) + s(n)$ to obtain the IMF $z_+(n)$. Similarly obtain $z_-(n)$ from $y_-(t_k) = y(t_k) - s(n)$.
3) Define the IMF as $z(n) = (z_+(n) + z_-(n))/2$.

The challenge with this method is the choice of the masking signal $s(n)$. How to select the frequency and amplitude of this new signal? According to [30], an appropriate choice would be to have each frequency within the signal separated by at least a factor of 2, is $s(n) = a_0 \sin(2\pi f_s t)$. Although some indications are given on how to choose a_0 and f_s, this process is usually empirical and the experience must guide the selection of parameters for a particular problem.

In [23], a strategy to calculate a_0 and f_s was proposed, based on the relation between the frequencies and amplitudes of each IMF. This new approach exploits the properties of the boundary map shown in Figure 1, which was previously developed in [8].

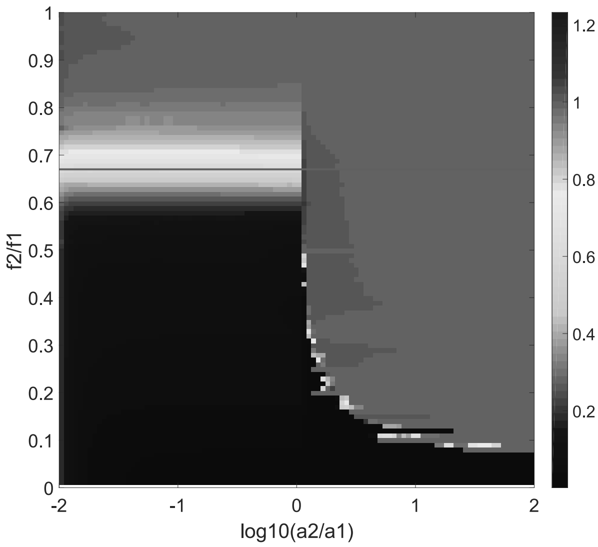

Fig. 1. Mode mixing boundary conditions map reproduced from [8] used for defining parameters of the masking signal

B. Ensemble Empirical Mode Decomposition

Wu and Huang proposed a noise-assisted data analysis (NADA), the Ensemble Empirical Mode Decomposition

(EEMD), which defines the true IMF components as the mean of an ensemble of trials, each consisting of the signal plus a white noise of finite amplitude [7]. The EEMD is described as:

1) Add a white noise series to the data base $y(t_k)$.
2) Decompose the data with added white noise using EMD to obtain the IMFs.
3) Repeat step 1 and step 2 again, but with different white noise series each time.
4) Obtain the (ensemble) means of corresponding IMFs of the decompositions as the final result.

The main effect of the decomposition using the EEMD is that the added white noise series cancel each other in the final mean of the corresponding IMFs. Modified versions of the EEMD have been recently proposed. In [32], the authors proposed one variation of EEMD, a Complete Ensemble Empirical Mode Decomposition with Adaptive Noise (CEEMDAN), and an improvement of CEEMDAN can be found in [33].

IV. New Masking Signal Strategy

The new method applied is based on the combination of the technique presented by Kaiser and the Boundary Conditions Map presented by Flandrin [8]. The properties of the map of boundary conditions between well separated tones and mixed tones (Figure 1) guides the choice of the masking signal's frequency and amplitude. To be able to extract a frequency by applying this principle, the ratio of that frequency to the frequency of the masking signal, must be located in the red area of the Boundary Map (mode mixing area is higher than 0.67 and approaches 1.0), while the ratio of the next frequency should be located in the blue area of the map, where mode mixing does not occur. The amplitude ratios need to be adopted from the map, with a ratio that will ensure that the above conditions are preserved. It is therefore necessary to operate with a frequency sufficiently close to the first IMF mode and sufficiently distant from the next IMF mode, to be successful. The map illustrates well how closely spaced spectral tones attract each other in a mode mixing, the colors representing the mode mixing degree; red for mode mixing and blue for No-mode mixing. This same property is exploited in this new masking method for constructing effective masking signals to separate closely spaced spectral tones.

Assume a signal with the two frequencies f_1 and f_2 ($f_1 > f_2$), where the ratio between them will cause mode mixing due to spectral proximity. A masking signal of frequency f_m larger than f_1 will attract f_1 if the ratio f_1/f_m falls into the attraction region of the map (red color). If the ratio between f_2/f_m falls in the region where there is no attraction (bluecolor), adding a positive masking signal of frequency f_m will separate the two signals f_1 and f_2 and the first IMF will have a controlled mode mixing of the signals f_1 and f_m. To separate f_1 and f_m a negative masking signal may be added, and by averaging the two first IMFs, the new IMF will be a signal of frequency f_1. However, depending on how close the two frequencies f_1 and f_2 are, some amplitude modulation may be observed between the signals f_1 and f_2. A way of identifying the frequencies involved in the original signal, is to process a Fast Fourier Transform (FFT) of the signal. In [23], a technique has been developed to identify the involved instantaneous frequencies and amplitudes, to assist in choosing the right masking signal. Assume a signal x defined by:

$$x = A\sin(2\pi f_1 t) + B\sin(2\pi f_2 t) \tag{3}$$

After EMD is performed, these two signals will be mixed into one IMF if they are sufficiently close in frequency. A Hilbert-transform of the mode mixed IMF ($s = x + jy$) followed by an amplitude and an instantaneous frequency calculation, will provide the required information for identifying the amplitudes and frequencies of the two signals involved. The instantaneous frequency used here is defined by:

$$f = \frac{1}{2\pi}\frac{\partial\phi}{\partial t}, \tag{4}$$

where $\tan\phi = (y/x)$ and $\phi = \arctan(y/x)$.

Using this definition, the equations for the amplitudes and the instantaneous frequencies can be derived. The amplitudes of the Hilbert-transformed signal are given by:

$$K = \sqrt{A^2 + B^2 + 2AB\cos(2\pi(f_1 - f_2)t)} \tag{5}$$

From this equation, the following expressions for the extreme values can be derived:

$$K_{min} = \sqrt{A^2 + B^2 - 2AB} = (A - B) \tag{6}$$

$$K_{max} = \sqrt{A^2 + B^2 + 2AB} = (A + B) \tag{7}$$

Similarly, the equation for the instantaneous frequencies are given by:

$$f = \frac{A^2 f_1 + B^2 f_2 + AB(f_1 + f_2)\cos(2\pi(f_1 - f_2)t)}{A^2 + B^2 + 2AB\cos(2\pi(f_1 - f_2)t)} \tag{8}$$

The expressions obtained for the extreme values are:

$$F_{min} = \frac{A\Delta f}{(A + B)} + f_2 \tag{9}$$

$$F_{max} = \frac{A\Delta f}{(A - B)} + f_2 \tag{10}$$

where, K_{min} is the Minimum value of the amplitude plot, K_{max} is the Maximum value of the amplitude plot, F_{min} is the Minimum value of the instantaneous frequency plot, F_{max} is the Maximum value of the instantaneous frequency plot and Δf is the difference between the two frequencies ($f_1 - f_2$).

It is also demonstrated that Δf is equal to the number of peaks/second in the instantaneous frequency and the amplitude plots. The frequencies f_1 and f_2 can now be calculated and may be further validated with a FFT calculation. In the case of synthetic signals, these calculations are accurate and in principle the signal components could have been obtained directly by applying the above presented analytical technique. However, for real signals the instantaneous amplitude and frequency functions are less smooth, but still this procedure will reveal information about the amplitudes and frequencies involved in the different periods of a mode mixed signal. From this information, an optimal masking signal based on the boundary map can be constructed. The process of extracting the IMFs is illustrated in the flowchart of Figure 2. An iterative procedure is used where the IMFs are extracted one by one by using the previously described procedure for optimal design of a masking signal. After the first IMF is extracted and accepted as an intrinsic mode, the residue ($s_{n+1}(t)$) of the signal is used in the next iteration. The acceptance of the IMF is decided by observation of the obtained first IMF instantaneous frequency profile and depends on the user experience and his a-priory knowledge of the studied system. The next iteration consists on performing a new EMD and again observing the first IMF instantaneous frequency profile. This profile will provide a hint about the presence of mode mixing. Once the frequencies involved in the mode mixing are identified, a new masking signal is designed according to the procedure above described. After the masking method is applied, the second IMF of this iterative process will be obtained. Once this second IMF is accepted, a new residue of the signal will be calculated by subtracting the two accepted IMFs from the original signal. This new residue will then be used in the next iteration. Iterations will be stopped once mode mixing is not detected anymore. The last residue in that case will contain the last IMF and/or the final residue of the EMD process.

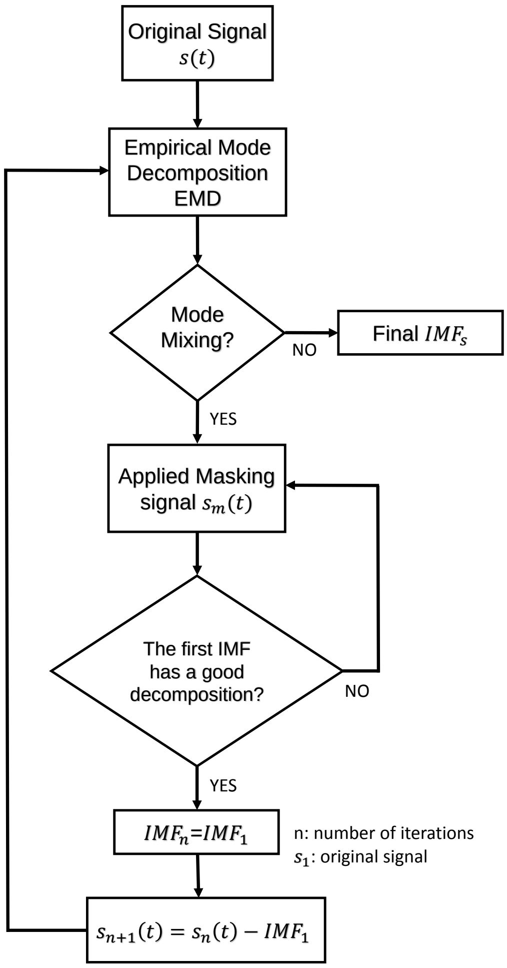

Fig. 2. Flowchart of the iterative process for IMFs extraction in the presence of Mode Mixing

V. Illustrative Examples

In order to evaluate the behavior of the methods presented in section III and IV, three databases for EEG generation are used. For the first and second databases the objective is to be able to observe in each IMF, neural activities at different frequencies. For the third database the objective is to obtain in one IMF the relevant activity (alpha band). The use of simulated databases for EEG source localization is a common approach for evaluation of brain mapping methods since the underlying source activity is known, and therefore, having a benchmark it is possible to evaluate the quality of the brain activity estimation.

The first simulated database (DB-1) contains neural activity $\boldsymbol{x}(t_k)$ by considering temporal localized sinusoidal signals with two different frequencies (6Hz and 8Hz) by using a Gaussian window, with sampling rate of 100Hz. In this case, two sources randomly located into the brain are selected, where the activity in each source is generated according to the following expression:

$$x_i(t_k) = e^{-\frac{1}{2}\left(\frac{t_k - c_i}{\sigma}\right)^2} \sin(2\pi f_i t_k) \tag{11}$$

being c_i the center of the windowed signal in seconds, and f_i the frequency of the signal, with $i = 1, 2$. The c_i is selected in the following ranges $c_i : [0.5, 3.5]$ seconds. The second simulated database (DB-2) uses the same model shown in (11) but with three different frequencies (4Hz, 8Hz and 10Hz). In DB-1 and DB-2, we have considered information from 30 channels.

The third simulated database (DB-3) contains neural activity generated by two sources randomly located into the brain with activity $\boldsymbol{x}(t_k)$ in the range of 8Hz to 13Hz, with sampling rate of 100Hz. The time of the two distinguished sources in the vector $\boldsymbol{x}(t_k)$ are modeled using bivariate linear auto-regressive (AR) models with time-delayed linear influences from one source to another. Sources are bandpass-filtered in the alpha band using a causal third-order Butterworth filter with zero phase delay. The generated time series therefore represent alpha oscillations that are either mutually statistically independent or characterized by a clearly defined sender-receiver relationship. In addition, 500 mutually statistically independent brain noise time series characterized by 1 / f-shaped (pink noise) power and random phase spectra are generated, and placed randomly at 500 locations sampled from the entire cortical surface [34]. In DB-3, we have considered information from 108 channels.

For DB-1 and DB-2, the EEG signals are obtained as a linear combination of the underlying neural activity as follows:

$$\boldsymbol{y}(t_k) = \boldsymbol{M}\boldsymbol{x}(t_k) + \boldsymbol{\epsilon}(t_k) \tag{12}$$

being $\boldsymbol{y}(t_k) \in \mathbb{R}^d$ the EEG signal measured at each electrode on the scalp, and $\boldsymbol{x}(t_k) \in \mathbb{R}^n$ the neural activity or amplitude of n current dipoles (distributed sources inside the brain), with $t_k = kh$ the time at sample k being $k = 1, \ldots, T$ the total number of samples, h the sample time and $\boldsymbol{M} \in \mathbb{R}^{d \times n}$ the lead-field matrix that relates the neural activity with the

EEG. Specifically, each row of the lead-field matrix describes the current flow for a given electrode through each dipole position [35]. Here, the Gaussian additive noise is defined by (ϵ). A Signal-to-Noise-Ratio (SNR) of 10dB is used for both databases.

For the DB-1 and DB-2, the lead field matrix is described in [36] based on a Boundary Element Method with a high number of distributed sources $n = 20484$ and $d = 30$ electrodes over the scalp according to a 10-20 standard BIOSEMI [37]. Positions of electrodes and sources are shown in Fig. 3.

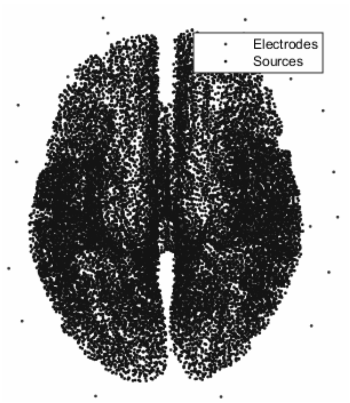

Fig. 3. Positions of electrodes and distributed sources for DB-1 and DB-2

Figure 4 shows the simulated DB-1 neural activity and source locations for the two different frequencies (6Hz and 8Hz) at two different positions into the brain and the corresponding EEG, with $f_1 = 6$Hz, $f_2 = 8$Hz, $c_1 = 1$ s, $c_2 = 2$ s and $\sigma = 0.12$.

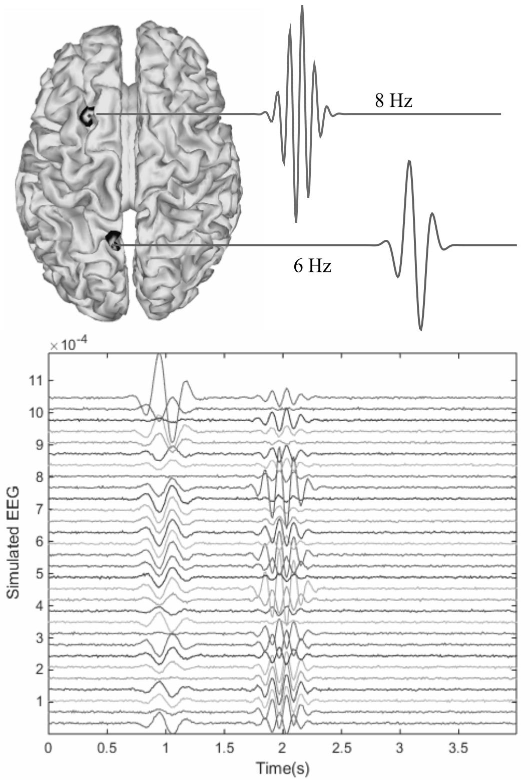

Fig. 4. Neural Activity of simulated DB-1 with their corresponding source locations and simulated EEG.

Figure 5 shows the Fourier spectrum of one channel for DB-1 and DB-2. In this figure it is possible to see that different frequencies appear but they are not appropriate to determine at which instant of time they occur.

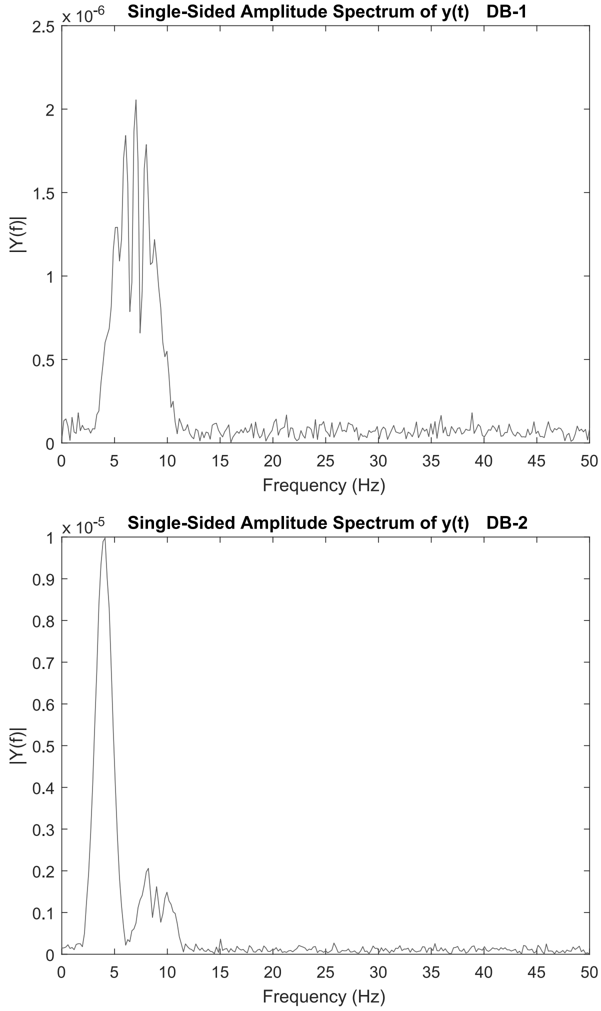

Fig. 5. Fourier spectrum for one channel using DB-1 and DB-2.

For the DB-3, the lead-field matrix is obtained from the so-called New York Head model as used in [34], which combines a highly detailed magnetic resonance (MR) image of an average adult human head with state-of-the-art finite element electrical modeling. In particular, the New York Head model holds $n = 2004$ sources and $d = 108$ electrodes.

Figure 6 shows the simulated DB-3 neural activity and source locations for the two different sources and their locations into the brain with their corresponding EEG.

Figure 7 shows the Fourier spectrum of one channel of DB-3.

The brain activity estimation is performed by using a dynamic inverse problem considering that only the EEG $\boldsymbol{y}(t_k)$ and the lead-field matrix $\boldsymbol{M}$ are known. The dynamic inverse problem of brain activity estimation $\widehat{\boldsymbol{x}}(t_k)$ can be formulated, according to [36], as:

$$\widehat{\boldsymbol{x}}(t_k) = \arg\min_{\boldsymbol{x}(t_k)} \|\boldsymbol{y}(t_k) - \boldsymbol{M}\boldsymbol{x}(t_k)\|_2^2 + \lambda_k \|\boldsymbol{x}(t_k) - \widehat{\boldsymbol{x}}(t_{k-1})\|_2^2 + \alpha_k \|\boldsymbol{x}(t_k)\|_1 \tag{13}$$

where λ_k and α_k are the regularization parameters computed by generalized cross validation. It can be noticed that as

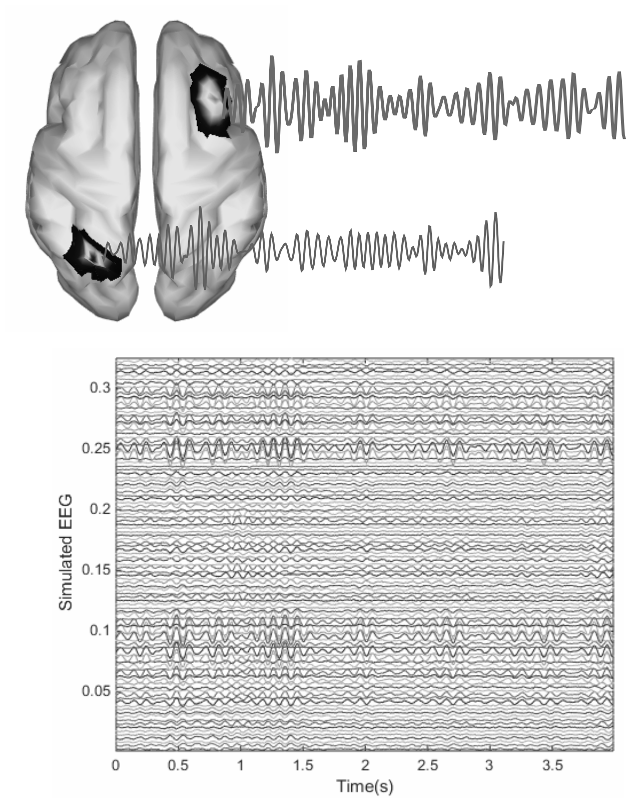

Fig. 6. Neural Activity of simulated DB-3 with their corresponding source locations and simulated EEG.

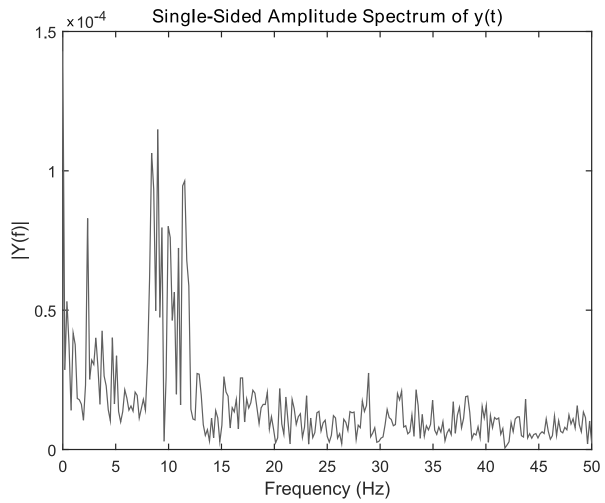

Fig. 7. Fourier spectrum for one channel using DB-3.

a result of the EMD decomposition, the brain activity estimation of $\boldsymbol{x}(t_k)$ can be obtained for each one of the resulting IMFs. That means that according to (1), the dynamic inverse problem of (13) is solved for $\boldsymbol{\gamma}_i(t_k)$ instead of $\boldsymbol{y}(t_k)$, as described in [38], as follows

$$\begin{aligned}\widehat{\chi}_i(t_k) = \arg\min_{\chi(t_k)} &\|\gamma_i(t_k) - \boldsymbol{M}\chi_i(t_k)\|_2^2 \\ &+ \lambda_k \|\chi_i(t_k) - \widehat{\chi}_i(t_{k-1})\|_2^2 \\ &+ \alpha_k \|\chi_i(t_k)\|_1\end{aligned} \tag{14}$$

where $\chi_i(t_k)$ is the neural activity estimation for the corresponding IMF $\gamma_i(t_K)$. In addition, as shown in (12), the forward problem of EEG generation is a linear problem, then it can be seen that $\boldsymbol{x}(t_k)$ can be rewritten as a linear combination of the estimated neural activity for each IMF $\boldsymbol{x}(t_k) = \sum_{i=1}^{N} \chi_i(t_k)$. Therefore, equation (14) is a sub-band brain mapping based on an EMD decomposition. Finally, Fig. 8 shows the methodology used, which starts with the decomposition of the EEG using three different methods to finally do the mapping of the neural activity.

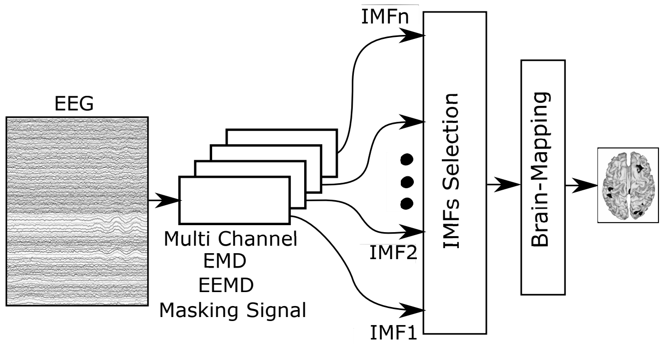

Fig. 8. Schematic representation of the methodology with its different stages

A. Analysis for DB-1

The IMFs obtained for 1 of the 30 channels with the EMD proposed in [25] and the EEMD proposed in [7] are shown in Fig. 9. The decomposition obtained for one channel with the novel method proposed in this paper is shown in Figure 10. The noise standard deviation of EEMD is set to 0.1 in this work. According to the experiments carried out, the noise standard deviation is the most relevant parameter in this algorithm. The number of iterations had been set to 1000. This process is repeated for each channel and in this way, the IMFs are obtained for the entire database.

In this case, the results of EMD shows clear mode mixing in all the IMFs. In the first and second IMF, it is possible to observe the two frequency components (6Hz in t=1s and 8Hz in t=2s). In the first IMF, the frequency component of 6Hz appears more clearly. Normally, we would expect to find the highest frequency component,in this case 8Hz, in the first IMF. For the EEMD, it is possible to observe the frequency component for 6Hz and 8Hz in the first and second IMF respectively. The instantaneous frequency shows similar behavior with the EMD and the EEMD. In the instantaneous frequency corresponding to the first IMF of the EMD, it is possible to distinguish one frequency component around t=1s and other frequency component around t=2s. In the EEMD, it is possible to distinguish one frequency component around t=2s. However, although it is possible to identify the frequencies of our interest, some other elements are observed, especially in the IMF1; these elements correspond to noise components. The results obtained with the new masking signal method, allow us to observe a better decomposition of the signal. In Figure 10, it is possible to see how the signal of one-channel EEG is decomposed correctly in 3 IMFs. At the top of the figure, the original signal appears. In the first IMF, the noise component is well isolated and in the remaining IMFs, the expected two frequency components are clearly identified. Figure 11 shows a comparison among the proposed methods by using the neural activity mapping for the first two IMFs for DB-1. It can be seen that in the

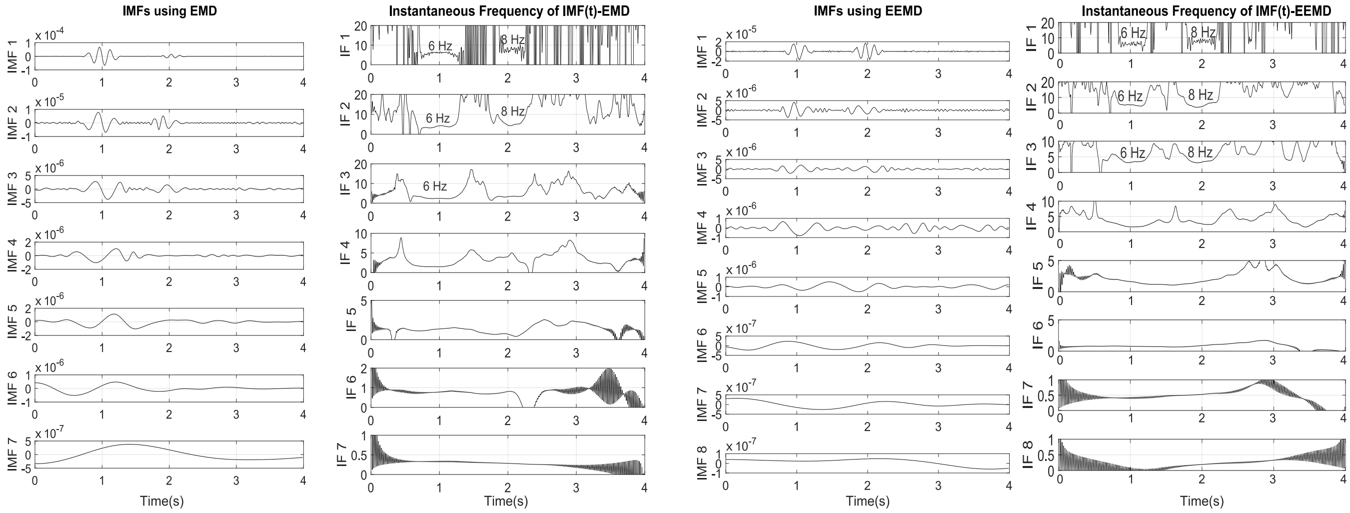

Fig. 9. IMFs and Instantaneous Frequency with EMD and EEMD using DB-1

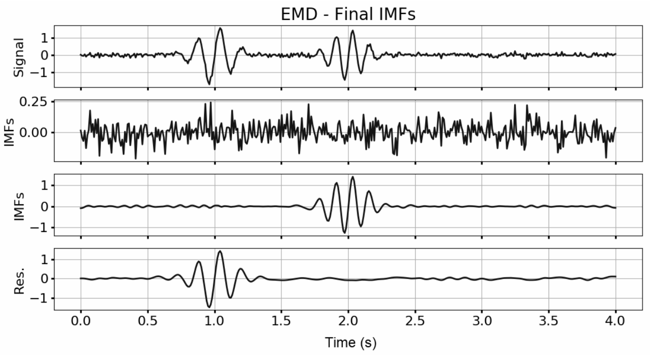

Fig. 10. IMFs with EMD+Mask using DB-1

first IMF, the EMD with a Mask has less spurious activity than the standard EMD and EEMD in comparison with the Ground truth.

B. Analysis for DB-2

The IMFs obtained for 1 of the 30 channels with the EMD proposed in [25] and the EEMD proposed in [7] are shown in Fig. 12. Finally the decomposition obtained with the novel method proposed in this paper is shown in Figure 13.

In this case, the results of EMD shows clear mode mixing in all the IMFs. In the second and third IMF, it is possible to observe the three frequency components (4Hz in t=1s, 8Hz in t=2s and 10Hz in t=3s). The first IMF corresponds to the noise of the signal. For the EEMD is possible to observe all the information of interest in the second and third IMFs, where the second IMF is one clear case of mode mixing. The instantaneous frequency has a similar behavior with the EMD and the EEMD. In the instantaneous frequency corresponding to the second IMF of the EMD, it is possible to distinguish three frequency components around t=1s, t=2s and t=3s. In the EEMD, it is possible to distinguish two frequency components around t=2s and t=3s in the second IMF. The results obtained with the new masking signal method, allow us to observe a better decomposition of the signal. In Figure 13, it is possible to see how the signal of one-channel EEG is decomposed correctly in 3 IMFs. At the top of the figure, the original signal appears. In the first IMF, the noise component is well isolated and in the remaining IMFs the expected three frequency components are clearly identified.

Figure 14 shows a comparison among the proposed methods by using the neural activity mapping for the first two IMFs for DB-2. It can be seen that in the first IMF the EMD with a Mask has less spurious activity than the standard EMD and EEMD in comparison with the Ground truth.

C. Analysis for DB-3

The IMFs obtained for 1 of the 108 channels with the EMD proposed in [25] and the EEMD proposed in [7] are shown in Fig. 15. For this case, the decomposition obtained with the new masking signal is shown in Fig. 16.

The EMD and the EEMD have clear mode mixing in all the IMFs. However, the frequency components of our interest, 8 Hz and 13 Hz, appear in 2 of the 7 IMFs. The IMF1 in both cases corresponds to noise. In IF2 and IF3, it is possible to see two red lines that corresponds to the frequencies of 8 Hz and 13 Hz.

Fig. 17 shows a comparison among the proposed methods by using the neural activity mapping for the IMF2 and IMF3 for DB-3 (according to the IMFs instantaneous frequencies the IMF2 and IMF3 hold the relevant information). The reconstruction of neural activity in this case was very close to the ground truth.

VI. Discussion

The mode mixing problem has been studied in different fields and in most cases the suggested solution has been to address the problem by using EEMD or to a lesser extent a masking signal (the idea is to separate two components whose frequencies are close). Noteworthy is the fact that while EEMD has been conceived to solve the mode mixing problem caused by intermittency, it has been generally used to solve all types of mode mixing problems regardless of their origin. The new masking method presented in this paper is specifically designed to reduce the mode mixing problem caused by the presence of modes with close spectral proximity. The main challenge when using the masking signal is the selection of its amplitude and

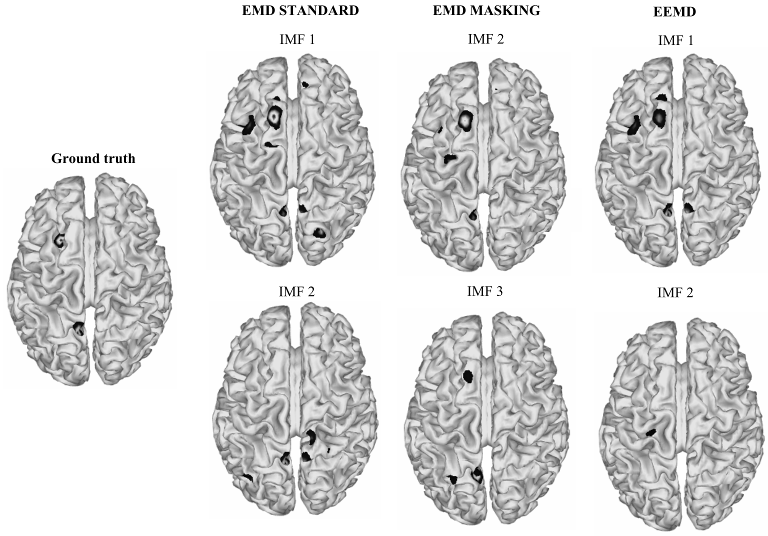

Fig. 11. Brain mapping comparison of the proposed methods for each IMFs for DB-1.

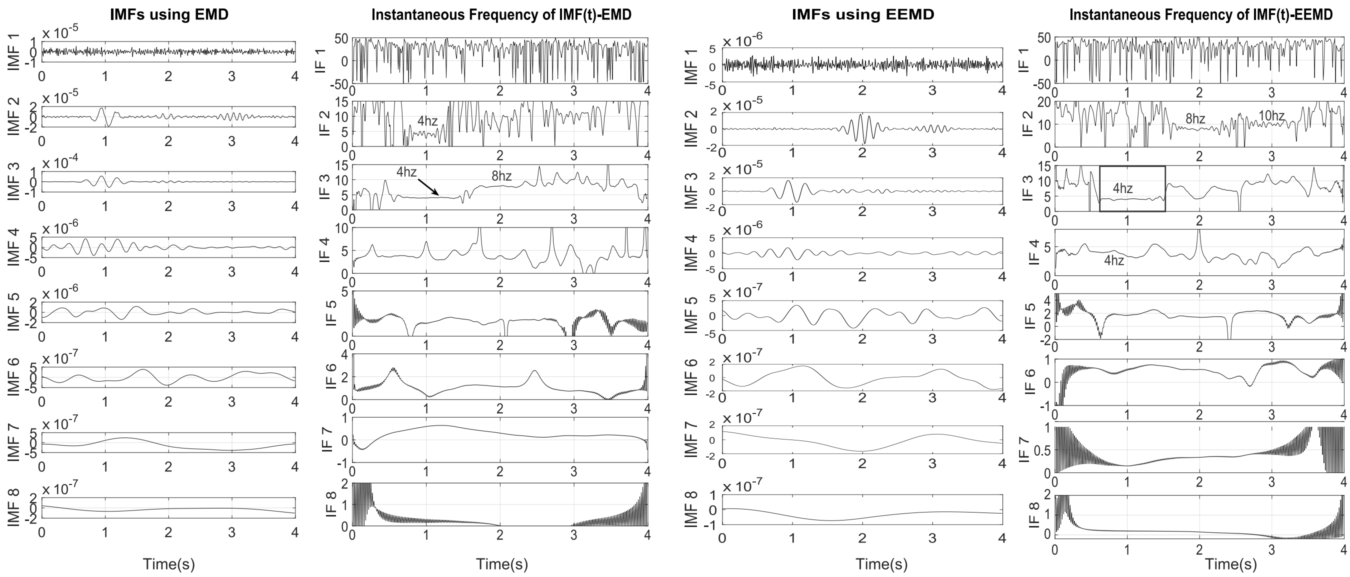

Fig. 12. IMFs and Instantaneous Frequency with EMD and EEMD using DB-2

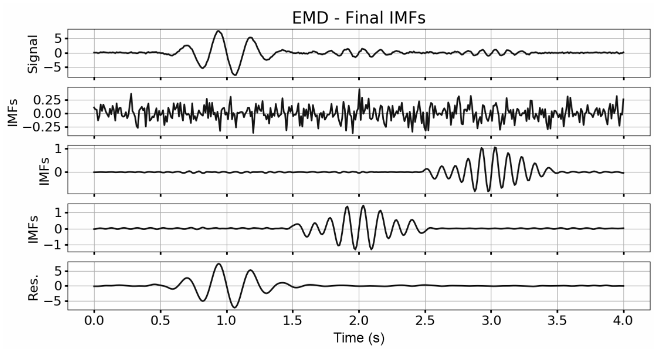

Fig. 13. IMFs with EMD+Mask using DB-2

frequency, but after selecting adequate values, the method shows to work very well. Another alternative that has been used to reduce mode mixing was to combine EMD or EEMD with some statistical method that allows to establish a criterion for selection of the IMFs according to the application. For example, in [39], the authors decompose EEG signal segments using EEMD, and then they extract statistical moment based features from the resulting IMFs. In [40], they proposed one technique to separate the sources from single-channel EEG signals by combining EEMD and Independent component analysis (ICA). For the case study in this paper, the objective is to show that it is possible to achieve an accurate mapping of neuronal activity using the IMFs obtained directly from the EMD with masking.

In Fig. 12, it is evident that the IMFs from the EMD have mode mixing. This is detected by observing different oscillations in the same IMF. As shown in Figures 11 and 14, it can be seen that the sub-band reconstruction effectively splits the brain activity into frequency bands. In fact, for signals with low SNR, it is clear that the noise is adaptively filtered in a specific IMF. However, a drawback of the method can be observed in the reconstructions obtained at low frequencies, where the activity is identifiable in several IMFs. On the other hand, the Instantaneous Frequency (IF) shown in Fig. 9, 12 and 15 is useful to detect instantaneous variations of the frequency. For EEG signals resulting from

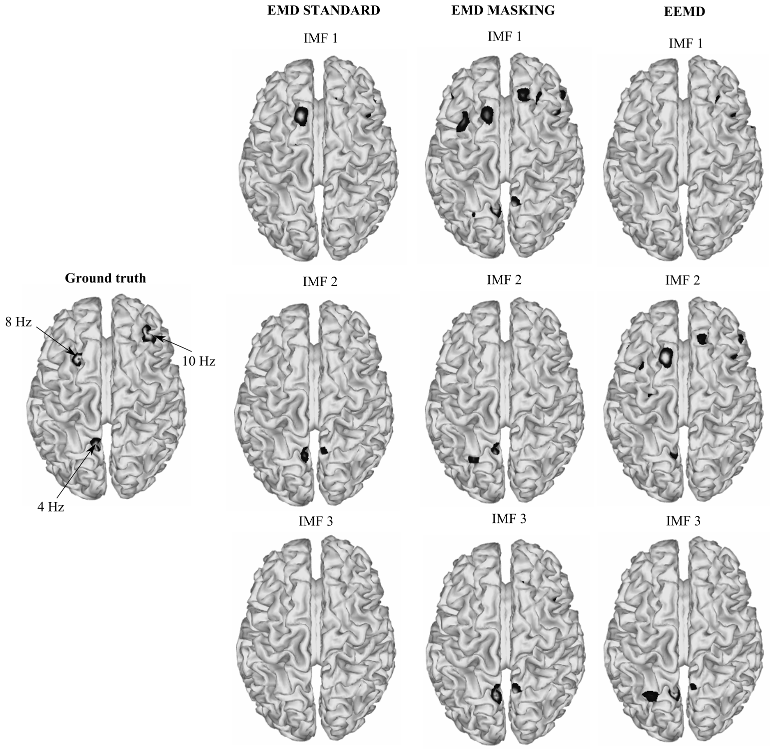

Fig. 14. Brain mapping comparison of the proposed methods for each IMFs for DB-2.

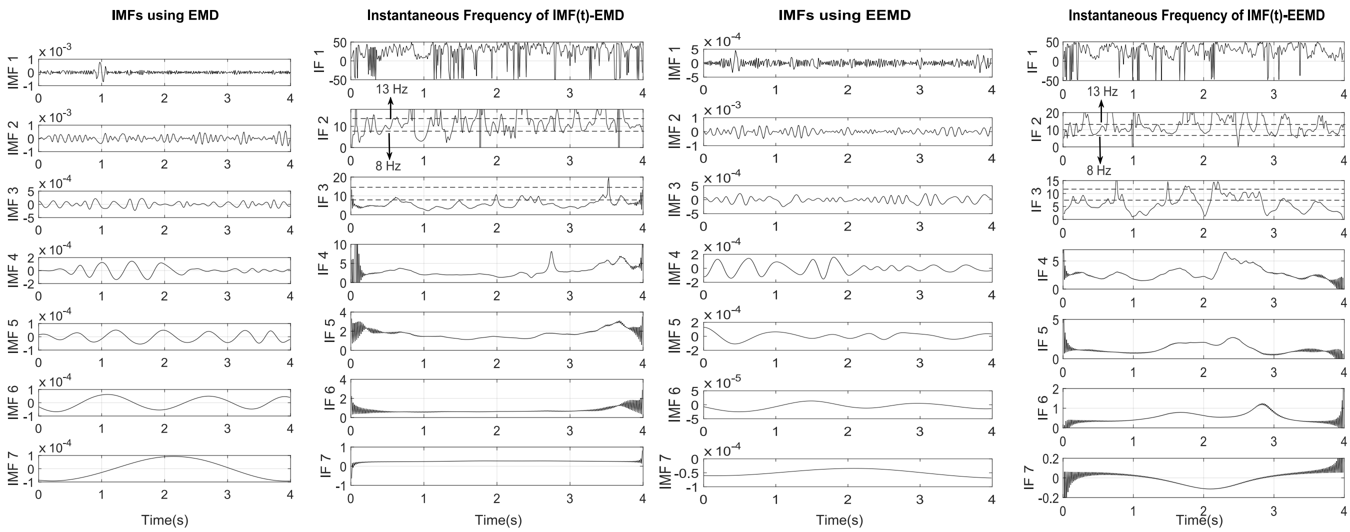

Fig. 15. IMFs and Instantaneous Frequency with EMD and EEMD using DB-3

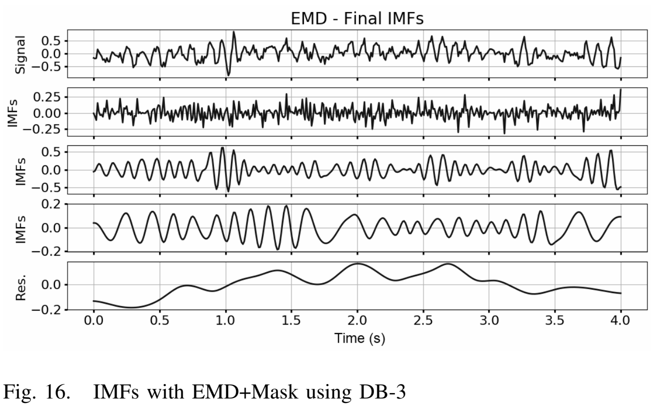

Fig. 16. IMFs with EMD+Mask using DB-3

Evoked-Related-Potentials or Epilepsy, the IF can be used to automatically detect the neural response to an external stimulus, or the beginning of an epileptic seizure. To improve the results with the new masking signal proposed, it is possible to use some statistical methods and combine the results of both strategies.

VII. Conclusions

In this paper, we have proposed a method for decomposing an EEG signal into a set of intrinsic mode functions (IMF) for mapping and reconstruction of the neuronal activity of the brain. The use of EMD is motivated by the fact that EEG signals are non-stationary and EMD is a data dependent method exhibiting a better adaptability towards the non-stationary nature of the EEG signals. The decomposition

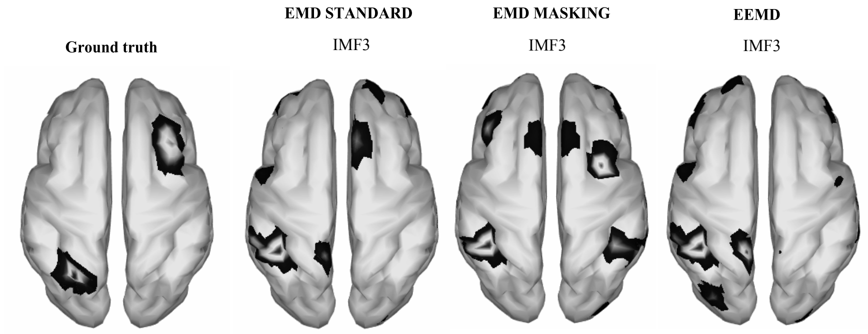

Fig. 17. Brain mapping comparison of the proposed methods for the IMF-4 for DB-3.

allows to identify behaviors in each of the frequency bands. Although the reconstruction has some undesirable components, the results show clearly the two sources where the activity was added in DB-1 and DB-2. For DB-3, it was possible to identify the frequency range of interest. Due to the mode mixing problem of EMD, it is possible that one frequency component appears in different bands, which is one of the drawbacks when using EMD. However, the results obtained show a significantly improved reconstruction of neural activity compared to conventional methods used for the same purpose. Future research efforts will be dedicated to the development of tools for mitigating the problem of mode mixing in EEG signals to obtain an even better sub-bands separation. The proposed methodology shows a clear potential to separate EEG signals in sub-bands that will facilitate the analysis of brain activity reconstruction, by adaptively separating noise from signals. In addition, based on the obtained results by applying a sub-band neural reconstruction, it can be seen that the reconstructed neural activity can be used for functional connectivity analysis by sub-bands, which implies a great potential of the proposed methodology as a tool for assisted diagnosis in brain related disorders. The case studies shown in this paper have allowed us to demonstrate that it is not always necessary to combine EMD or EEMD with some statistical method (energy or entropy function) to obtain a good reconstruction of the neuronal activity.

REFERENCES

[1] M. Soleymani, S. Asghari-Esfeden, Y. Fu, and M. Pantic, "Analysis of EEG signals and facial expressions for continuous emotion detection," *IEEE Transactions on Affective Computing*, vol. 7, no. 1, pp. 17–28, Jan 2016.

[2] K. Y. Lin, D. Y. Chen, and W. J. Tsai, "Face-based heart rate signal decomposition and evaluation using multiple linear regression," *IEEE Sensors Journal*, vol. 16, no. 5, pp. 1351–1360, March 2016.

[3] D. P. Subha, P. K. Joseph, R. Acharya U, and C. M. Lim, "EEG signal analysis: A survey," *Journal of Medical Systems*, vol. 34, no. 2, pp. 195–212, Apr 2010.

[4] R. Sukanesh and R. Harikumar, "A comparison of genetic algorithm & neural network (MLP) in patient specific classification of epilepsy risk levels from EEG signals," *Engineering Letters*, vol. 14, no. 1, pp. 96–104, 2007.

[5] ——, "A patient specific neural networks (MLP) for optimization of fuzzy outputs in classification of epilepsy risk levels from EEG signals," *Engineering Letters*, vol. 13, no. 2, pp. 50–56, 2006.

[6] ——, "Diagnosis and classification of epilepsy risk levels from eeg signals using fuzzy aggregation techniques," *Engineering Letters*, vol. 14, no. 1, pp. 90–95, 2007.

[7] Z. Wu and N. E. Huang, "Ensemble Empirical Mode Decomposition: A noise-assisted data analysis method," *Advances in Adaptive Data Analysis*, vol. 1, no. 1, pp. 1–41, 2009.

[8] G. Rilling and P. Flandrin, "One or two frequencies? The empirical mode decomposition answers," *IEEE Transactions on Signal Processing*, vol. 56, no. 1, pp. 85–95, Jan 2008.

[9] Y. juan Xue, J. xing Cao, H. kun Du, G. lan Zhang, and Y. Yao, "Does mode mixing matter in EMD-based highlight volume methods for hydrocarbon detection? experimental evidence," *Journal of Applied Geophysics*, vol. 132, no. Supplement C, pp. 193 – 210, 2016.

[10] B. Tang, S. Dong, and T. Song, "Method for eliminating mode mixing of empirical mode decomposition based on the revised blind source separation," *Signal Processing*, vol. 92, no. 1, pp. 248 – 258, 2012.

[11] W.-C. Shen, Y.-H. Chen, and A.-Y. A. Wu, "Low-complexity sinusoidal-assisted EMD (SAEMD) algorithms for solving mode-mixing problems in HHT," *Digital Signal Processing*, vol. 24, no. Supplement C, pp. 170 – 186, 2014.

[12] M. Bueno-López, P. A. Muñoz-Gutiérrez, E. Giraldo, and M. Molinas, "Analysis of epileptic activity based on brain mapping of eeg adaptive time-frequency decomposition," in *Brain Informatics*, S. Wang, V. Yamamoto, J. Su, Y. Yang, E. Jones, L. Iasemidis, and T. Mitchell, Eds. Cham: Springer International Publishing, 2018, pp. 319–328.

[13] P. Munoz-Gutiérrez, E. Giraldo, M. Bueno-López, and M. Molinas, "Localization of active brain sources from EEG signals using empirical mode decomposition: A comparative study," *Frontiers in Integrative Neuroscience*, vol. 12, no. 1, pp. 1–13, 2018.

[14] K. Zeng, D. Chen, G. Ouyang, L. Wang, X. Liu, and X. Li, "An EEMD-ICA approach to enhancing artifact rejection for noisy multivariate neural data," *IEEE Transactions on Neural Systems and Rehabilitation Engineering*, vol. 24, no. 6, pp. 630–638, June 2016.

[15] S. Kar and A. Routray, "Effect of sleep deprivation on functional connectivity of EEG channels," *IEEE Transactions on Systems, Man, and Cybernetics: Systems*, vol. 43, no. 3, pp. 666–672, May 2013.

[16] V. Bajaj and R. B. Pachori, "Classification of seizure and nonseizure EEG signals using empirical mode decomposition," *IEEE Transactions on Information Technology in Biomedicine*, vol. 16, no. 6, pp. 1135–1142, Nov 2012.

[17] J. Molvaer and F. Worren, "A unified real-time feature extraction and classification process for a BCI based on empirical mode decomposition and support vector machine," Master's thesis, Norwegian University of Science and Technology, Trondheim, Norway, 2016.

[18] S. Alam and M. Bhuiyan, "Detection of seizure and epilepsy using higher order statistics in the EMD domain," *IEEE Journal of Biomedical and Health Informatics*, vol. 17, no. 2, pp. 312–318, March 2013.

[19] Q. Wei, Q. Liu, S.-Z. Fan, C.-W. Lu, T.-Y. Lin, M. F. Abbod, and J.-S. Shieh, "Analysis of EEG via multivariate empirical mode decomposition for depth of anesthesia based on sample entropy," *Entropy*, vol. 15, no. 9, pp. 3458–3470, 2013.

[20] A. Karagiannis and P. Constantinou, "Noise-assisted data processing with empirical mode decomposition in biomedical signals," *IEEE*

Transactions on Information Technology in Biomedicine, vol. 15, no. 1, pp. 11–18, Jan 2011.

[21] S. Qing-shan, M. Yu-liang, M. Ming, X. Xu-gang, and L. Zhi-zeng, "Noise-assisted MEMD based relevant IMFs identification and EEG classification," *Journal of Central South University*, vol. 24, no. 1, pp. 599–608, April 2017.

[22] D. Chen, D. Li, M. Xiong, H. Bao, and X. Li, "GPGPU-aided ensemble empirical-mode decomposition for EEG analysis during anesthesia," *IEEE Transactions on Information Technology in Biomedicine*, vol. 14, no. 6, pp. 1417–1427, Nov 2010.

[23] O. Fosso and M. Molinas, "Method for mode mixing separation in empirical mode decomposition," *eprint arXiv:1709.05547*, pp. 1–7, 2017.

[24] V. Gonuguntla, Y. Wang, and K. C. Veluvolu, "Event-related functional network identification: Application to EEG classification," *IEEE Journal of Selected Topics in Signal Processing*, vol. 10, no. 7, pp. 1284–1294, Oct 2016.

[25] N. E. Huang, Z. Shen, S. R. Long, M. C. Wu, H. H. Shih, Q. Zheng, N.-C. Yen, C. C. Tung, and H. H. Liu, "The empirical mode decomposition and the Hilbert spectrum for nonlinear and non-stationary time series analysis," *Proceedings of the Royal Society of London A: Mathematical, Physical and Engineering Sciences*, vol. 454, no. 1971, pp. 903–995, 1998.

[26] D. P. Mandic, N. U. Rehman, Z. Wu, and N. E. Huang, "Empirical mode decomposition-based time-frequency analysis of multivariate signals: The power of adaptive data analysis," *IEEE Signal Processing Magazine*, vol. 30, no. 6, pp. 74–86, Nov 2013.

[27] D. Xu, Y. Xia, and D. P. Mandic, "Optimization in quaternion dynamic systems: Gradient, hessian, and learning algorithms," *IEEE Transactions on Neural Networks and Learning Systems*, vol. 27, no. 2, pp. 249–261, Feb 2016.

[28] T. Y. Hou and Z. Shi, "Data-driven time-frequency analysis," *Applied and Computational Harmonic Analysis*, vol. 35, no. 2, pp. 284–308, Sept 2013.

[29] B. Boashash, "Estimating and interpreting the instantaneous frequency of a signal. Part 1: Fundamentals," *Proceedings of the IEEE*, vol. 80, no. 4, pp. 520–538, Apr 1992.

[30] R. Deering and J. F. Kaiser, "The use of a masking signal to improve empirical mode decomposition," in *Proceedings. (ICASSP '05). IEEE International Conference on Acoustics, Speech, and Signal Processing, 2005.*, vol. 4, March 2005, pp. iv/485–iv/488.

[31] G. Rilling, P. Flandrin, and P. Gonçalves, "On empirical mode decomposition and its algorithms," in *Proceedings of IEEE-EURASIP Workshop on Nonlinear Signal and Image Processing NSIP-03*, June 2003.

[32] M. E. Torres, M. A. Colominas, G. Schlotthauer, and P. Flandrin, "A complete Ensemble Empirical Mode Decomposition with adaptive noise," in *2011 IEEE International Conference on Acoustics, Speech and Signal Processing (ICASSP)*, May 2011, pp. 4144–4147.

[33] M. A. Colominas, G. Schlotthauer, and M. E. Torres, "Improved complete ensemble EMD: A suitable tool for biomedical signal processing," *Biomedical Signal Processing and Control*, vol. 14, pp. 19–29, 2014.

[34] S. Haufe and A. Ewald, "A simulation framework for benchmarking eeg-based brain connectivity estimation methodologies," *Brain Topography*, pp. 1–18, 2016.

[35] R. Grech, T. Cassar, J. Muscat, K. P. Camilleri, S. G. Fabri, M. Zervakis, P. Xanthopoulos, V. Sakkalis, and B. Vanrumste, "Review on solving the inverse problem in EEG source analysis," *Journal of NeuroEngineering and Rehabilitation*, vol. 5, no. 1, p. 25, Nov 2008. [Online]. Available: https://doi.org/10.1186/1743-0003-5-25

[36] E. Giraldo-Suarez, J. Martinez-Vargas, and G. Castellanos-Dominguez, "Reconstruction of neural activity from EEG data using dynamic spatiotemporal constraints," *International Journal of Neural Systems*, vol. 26, no. 07, pp. 1–15, 2016.

[37] P. Praamstra, "The biosemi headcap," Website, October 2003, https://www.biosemi.com/headcap.htm.

[38] M. Bueno-Lopez, E. Giraldo, and M. Molinas, "Analysis of neural activity from eeg data based on emd frequency bands," in *24th IEEE International Conference on Electronics, Circuits and Systems (ICECS)*, vol. 1. Batumi, Georgia: IEEE, December 2017, pp. 1–5.

[39] A. Rashik and M. Hassan, "Automated identification of sleep states from eeg signals by means of ensemble empirical mode decomposition and random under sampling boosting," *Computer Methods and Programs in Biomedicine*, vol. 140, pp. 201–210, March 2017.

[40] A. K. Maddirala and R. A. Shaik, "Separation of sources from single-channel eeg signals using independent component analysis," *IEEE Transactions on Instrumentation and Measurement*, vol. 67, no. 2, pp. 382–393, Feb 2018.